Available online at www.sciencedirect.com
ScienceDirect
Comput. Methods Appl. Mech. Engrg. 196 (2007) 4811–4822
Computer methods in applied mechanics and engineering
www.elsevier.com/locate/cma

A two-dimensional self-adaptive *hp* finite element method for the characterization of waveguide discontinuities. Part II: Goal-oriented *hp*-adaptivity

David Pardo [a,b], Luis E. García-Castillo [c,*,1,2], Leszek F. Demkowicz [b], Carlos Torres-Verdín [a]

[a] *Department of Petroleum and Geosystems Engineering, The University of Texas at Austin, 201 East 24th Street, ACES 4.102, Austin, TX 78712, USA*
[b] *ICES, The University of Texas at Austin, 201 East 24th Street, ACES 4.102, Austin, TX 78712, USA*
[c] *Departamento de Teoría de la Señal y Comunicaciones, Universidad Carlos III de Madrid, Escuela Politécnica Superior (Edificio Torres Quevedo), Avda. de la Universidad, 30, 28911 Leganés, Madrid, Spain*

Received 23 February 2007; accepted 18 June 2007
Available online 26 July 2007

Abstract

This is the second part of the work on the analysis of different types of rectangular waveguide discontinuities by using a fully automatic *hp*-adaptive finite element method.

In this paper, we describe a fully automatic *goal-oriented hp*-adaptive Finite Element (FE) strategy. The methodology produces exponential convergence rates in terms of an upper bound of a user-prescribed quantity of interest (in our case, the *S*-parameters) against the problem size (number of degrees of freedom).

Specifically, the *hp*-methodology is applied to a fifth-order microwave filter using a H-plane structure consisting on symmetric inductive irises. Numerical results illustrate the main differences between the energy-norm based and the goal-oriented based *hp*-adaptivity, when applied to rectangular waveguide structures. They also demonstrate the suitability of the goal-oriented *hp*-method for solving problems involving rectangular waveguide structures.

The goal-oriented self-adaptive *hp*-FEM provides more accurate results than those obtained with the Mode Matching method (a semi-analytical technique). At the same time, the *hp*-FEM provides the flexibility of modeling more complex waveguide structures possibly incorporating the effects of dielectrics, metallic screws, round corners, etc., which cannot be easily considered when using semi-analytical techniques.

Keywords: Finite element method; *hp*-adaptivity; Goal-oriented adaptivity; Rectangular waveguides; Waveguide discontinuities; *S*-parameters

1. Introduction

As it was mentioned in Part I [1], the accurate analysis and characterization of "waveguide discontinuities" is an important issue in microwave engineering (see e.g., [2,3]). Specifically, H-plane and E-plane rectangular waveguide discontinuities, which are the target of the presented work, play an important role in the communication systems working in the upper microwave and millimeter wave frequency bands.

A method based on *hp* Finite Elements, presented in Part I [1], seems to be a perfect tool for solving the waveguide discontinuity problem because:

- the method automatically refines the grid around the singularities,

* Corresponding author. Tel.: +34 91 6249171; fax: +34 91 6248749.
E-mail addresses: dzubiaur@gmail.com (D. Pardo), luise.garcia@uah.es, luise@tsc.uc3m.es (L.E. García-Castillo), leszek@ices.utexas.edu (L.F. Demkowicz), cverdin@uts.cc.utexas.edu (C. Torres-Verdín).
[1] The author acknowledges the support of Ministerio de Educación y Ciencia of Spain under project TEC2004-06252/TCM.
[2] On leave from Departamento de Teoría de la Señal y Comunicaciones, Universidad de Alcalá, Madrid, Spain.

0045-7825/$ - see front matter © 2007 Elsevier B.V. All rights reserved.
doi:10.1016/j.cma.2007.06.023

- the method automatically increases the polynomial order of approximation in regions where the solution is smooth, and,
- the overall convergence of the method is fast (exponential convergence).

It is critical to notice that the exponential convergence of the *hp*-method described in [1] is measured in terms of the energy-norm of the error function against the problem size. Thus, the electromagnetic field is accurately known (with a user pre-specified level of accuracy) inside of the structure. This may be useful to the microwave engineer in order to predict the location and size of tuning elements (e.g., screws, dielectric posts, etc.) and/or for the design of modifications to the original design. However, the microwave engineer is first (and mainly) interested in accurately computing the *S*-parameters (see [1] for details) of the waveguide structure. Therefore, we should design a numerical method that is consistent with our goal, i.e., a high accuracy computation of the *S*-parameters, regardless of the quality of the solution in the rest of the domain.[3] This type of methods are called weighted-based residual methods or goal-oriented methods (see [4–9] for details).

At the same time, we would like to maintain all desirable properties (such as exponential convergence) of the self-adaptive *hp*-FEM described in [1].

In this work, we propose to use the fully automatic goal-oriented *hp*-FEM presented in [10–12] to compute the *S*-parameters of rectangular waveguide structures. This method incorporates all desirable features mentioned above with the additional advantage of obtaining exponential convergence in terms of a sharp upper bound of the quantity of interest (in this case, the *S*-parameters) against the problem size – number of degrees of freedom. In this paper, we consider the application of this goal-oriented methodology to a rectangular (H-plane) waveguide structure with six inductive irises. It is worth noting that this structure incorporates as many as 24 singularities of different intensity, due to presence of re-entrant corners in the geometry.

The organization of the paper is as follows. In Section 2, we describe our numerical methodology based on the self-adaptive goal-oriented *hp*-FEM. The variational formulation together with relevant properties of the quantities of interest are shown first. Following [10,11], we present the main ideas that make the practical use of goal-oriented adaptivity possible. Then, we introduce the projection based interpolation operator for 2D edge elements, which is a key component of the *hp* goal-oriented mesh optimization algorithm that is presented thereafter. A brief discussion on implementation details is also provided at this point. Section 3 is devoted towards numerical results. We introduce first the problem of interest in Section 3.1. Then, main advantages and disadvantages of using the goal-oriented *hp*-adaptivity (as opposed to the energy-norm *hp*-adaptivity) for our problem of interest are carefully analyzed. Finally, we close with some conclusions in Section 4.

[3] For instance, it may be unnecessary to resolve all singularities in order to accurately compute the *S*-parameters.

2. A fully automatic goal-oriented *hp*-adaptive finite element method

In this Section, we present the self-adaptive goal-oriented *hp*-FE method. The algorithm is an extension of the energy-norm based *hp*-adaptive FE method presented in [1].

2.1. Variational formulation and goals

We consider the variational formulation presented in Part I [1]. For convenience, it is briefly reviewed here serving also as an introduction to the notation used in the remainder of the paper. Specifically, the H-plane formulation is shown since is the one used to obtain the numerical results presented later in Section 3.

We excite the TE_{10}-mode at one of the ports of the H-plane structure. As explained in [1], the original 3D problem can be reduced to a 2D boundary value problem, which we can formulate in terms of the components of the magnetic field parallel to the H-plane (denoted by $\mathbf{H}_\Omega$) as follows:

$$\begin{cases} \nabla \times \left(\frac{1}{\epsilon}\nabla \times \mathbf{H}_\Omega\right) - \omega^2\mu\mathbf{H}_\Omega = 0 & \text{in } \Omega, \\ \hat{\mathbf{n}} \times \frac{1}{\epsilon}\nabla \times \mathbf{H}_\Omega = \frac{\mathrm{j}\omega^2\mu}{\beta_{10}}\hat{\mathbf{n}} \times \hat{\mathbf{n}} \times (2\mathbf{H}^{\text{in}} - \mathbf{H}_\Omega) & \text{on } \Gamma_1, \\ \hat{\mathbf{n}} \times \frac{1}{\epsilon}\nabla \times \mathbf{H}_\Omega = -\frac{\mathrm{j}\omega^2\mu}{\beta_{10}}\hat{\mathbf{n}} \times \hat{\mathbf{n}} \times \mathbf{H}_\Omega & \text{on } \Gamma_2, \\ \hat{\mathbf{n}} \times \frac{1}{\epsilon}\nabla \times \mathbf{H}_\Omega = \mathbf{0} & \text{on } \Gamma_3, \end{cases} \tag{1}$$

which is a particularization of expressions of [1]; specifically, Eqs. (6) and (7)–(9).

In (1), Γ_1, Γ_2, and Γ_3 stand for the parts of the boundary corresponding to the excitation port, non-excitation port, and the perfect electric conductor, respectively. That is, the formulation has been reduced to the case of a two ports structure; the Cauchy boundary condition at the ports has been expressed for the case of excitation port and non-excitation port. Note that no perfect magnetic conductors, i.e., Dirichlet boundary conditions (used to implement symmetry planes) have been considered. The symbol β_{10} refers to the propagation constant of the TE_{10} mode; $\mathbf{H}^{\text{in}}$ is the incident magnetic field at the excitation port; ω is the angular frequency; μ and ϵ are the magnetic permeability and the dielectric permittivity of the media, respectively; $\hat{\mathbf{n}}$ is the unit normal (outward) vector; and $\mathrm{j} = \sqrt{-1}$ is the imaginary unit.

The corresponding variational formulation is given by

$$\begin{cases} \text{Find } \mathbf{H}_\Omega \in \mathbf{H}_D(\text{curl};\Omega) \text{ such that} \\ \int_\Omega \frac{1}{\epsilon}(\nabla \times \mathbf{H}_\Omega) \cdot (\nabla \times \overline{\mathbf{F}}_\Omega)\mathrm{d}V - \int_\Omega \omega^2\mu\mathbf{H}_\Omega \cdot \overline{\mathbf{F}}_\Omega \mathrm{d}V \\ \quad + \frac{\mathrm{j}\omega^2\mu}{\beta_{10}} \int_{\Gamma_1 \cup \Gamma_2} (\hat{\mathbf{n}} \times \mathbf{H}_\Omega) \cdot (\hat{\mathbf{n}} \times \overline{\mathbf{F}}_\Omega)\mathrm{d}S \\ \quad = 2\frac{\mathrm{j}\omega^2\mu}{\beta_{10}} \int_{\Gamma_1} (\hat{\mathbf{n}} \times \mathbf{H}^{\text{in}}) \cdot (\hat{\mathbf{n}} \times \overline{\mathbf{F}}_\Omega)\mathrm{d}S \\ \quad \text{for all } \mathbf{F}_\Omega \in \mathbf{H}_D(\text{curl};\Omega). \end{cases} \tag{2}$$

In the above, $\mathbf{H}(\mathrm{curl};\Omega)$ is the Hilbert *space of admissible solutions*

$$\mathbf{H}(\mathrm{curl};\Omega) := \{\mathbf{H}_\Omega \in \mathbf{L}^2(\Omega) : \mathrm{curl}\mathbf{H}_\Omega \in L^2(\Omega)\}.$$

In the remainder of this paper, we shall work with 2D vectors, and we shall use the symbol $\mathbf{H}$ when referring to $\mathbf{H}_\Omega$ (components of the magnetic field parallel to the H-plane). Similarly, we will use symbol $\mathbf{F}$ when referring to $\mathbf{F}_\Omega$.

It is worth noting that the final objective of the computations is not to accurately determine $\mathbf{H}$ but the scattering parameters S_{ij} $(1 \leqslant i,j \leqslant 2)$ (see [1] for details on S-parameters). Thus, the quantity of interest (scattering parameters) for a two-ports waveguide consists of four complex numbers: S_{ij} $(1 \leqslant i,j \leqslant 2)$. Because of the reciprocity principle, we know that

$$S_{12} = S_{21}. \tag{3}$$

We also know that

$$S_{11} = S_{22} \tag{4}$$

for symmetric structures.

For a loss-less media, the S-matrix of the structure is unitary. Thus, we have

$$S_{11}^2 = S_{21}^2 - \frac{S_{21}}{\overline{S}_{21}}, \tag{5}$$

where $\overline{S}_{21}$ is the complex conjugate of S_{21}. Therefore, one of the S-parameters is enough to determine the full scattering matrix. Also, for loss-less media, $|S_{11}| = |S_{22}|$ in a two ports structure. The phases are equal only if there is symmetry (which means (3) holds).

This problem may be solved by using semi-analytical techniques (for example, Mode Matching techniques [13,14, Chapter 9]). Nevertheless, it would be desirable to solve it by using purely numerical techniques, since a numerical method allows for simulation of more complex geometries and/or the effects of dielectrics, metallic screws, round corners, etc., possibly needed for the construction of an actual waveguide.

2.2. Goal-oriented adaptivity

Given a problem, a quantity of interest (in this case, the S-parameters), and a discretization tolerance error, the objective of the goal-oriented adaptivity is to construct, without any user interaction, an *hp*-grid containing a minimum number of unknowns, and such that the relative error in the quantity of interest is smaller than the (given) error tolerance.

Variational problem (2) can be stated here in terms of sesquilinear form b, and antilinear form f

$$\begin{cases} \text{Find } \mathbf{H} \in \mathbf{V} \\ b(\mathbf{H},\mathbf{F}) = f(\mathbf{F}) \quad \forall \mathbf{F} \in \mathbf{V}, \end{cases} \tag{6}$$

where

- $\mathbf{V} = H(\mathbf{curl};\Omega)$ is a Hilbert space.
- $f(\mathbf{F}) = 2\frac{\mathrm{j}\omega^2\mu}{\beta_{10}} \int_{\Gamma_1} (\hat{\mathbf{n}} \times \mathbf{H}^{\mathrm{in}}) \cdot (\hat{\mathbf{n}} \times \overline{\mathbf{F}}) \mathrm{d}S \in \mathbf{V}'$ is an antilinear and continuous functional on $\mathbf{V}$.
- b is a sesquilinear form. We have

$$\begin{aligned} b(\mathbf{H},\mathbf{F}) &= a(\mathbf{H},\mathbf{F}) + c(\mathbf{H},\mathbf{F}), \\ a(\mathbf{H},\mathbf{F}) &= \int_\Omega \frac{1}{\epsilon} (\nabla \times \mathbf{H}) \cdot (\nabla \times \overline{\mathbf{F}}) \mathrm{d}V \\ &\quad + \frac{\mathrm{j}\omega^2\mu}{\beta_{10}} \int_{\Gamma_1 \cup \Gamma_2} (\hat{\mathbf{n}} \times \mathbf{H}) \cdot (\hat{\mathbf{n}} \times \overline{\mathbf{F}}) \mathrm{d}S, \\ c(\mathbf{H},\mathbf{F}) &= -\int_\Omega \omega^2 \mu \mathbf{H} \cdot \overline{\mathbf{F}} \mathrm{d}V. \end{aligned} \tag{7}$$

We define an "energy" inner product on $\mathbf{V}$ as

$$\begin{aligned} &(\mathbf{H},\mathbf{F}) := \tilde{a}(\mathbf{H},\mathbf{F}) + \tilde{c}(\mathbf{H},\mathbf{F}), \\ &\tilde{a}(\mathbf{H},\mathbf{F}) = \int_\Omega \frac{1}{\epsilon} (\nabla \times \mathbf{H}) \cdot (\nabla \times \overline{\mathbf{F}}) \mathrm{d}V + \left|\frac{\mathrm{j}\omega^2\mu}{\beta_{10}}\right| \int_{\Gamma_1 \cup \Gamma_2} (\hat{\mathbf{n}} \times \mathbf{H}) \cdot (\hat{\mathbf{n}} \times \overline{\mathbf{F}}) \mathrm{d}S, \\ &\tilde{c}(\mathbf{H},\mathbf{F}) = \int_\Omega \omega^2 \mu \mathbf{H} \cdot \overline{\mathbf{F}} \mathrm{d}V \end{aligned} \tag{8}$$

with the corresponding (energy) norm denoted by $\|\mathbf{H}\|$. Notice the inclusion of the material properties in the definition of the norm.

Using high-order Nedelec (edge) elements [15], we consider an *hp*-FE subspace $\mathbf{V}_{hp} \subset \mathbf{V}$. Then, we discretize (6) as follows:

$$\begin{cases} \text{Find } \mathbf{H}_{hp} \in \mathbf{V}_{hp} \\ b(\mathbf{H}_{hp},\mathbf{F}_{hp}) = f(\mathbf{F}_{hp}) \quad \forall \mathbf{F}_{hp} \in \mathbf{V}_{hp}. \end{cases} \tag{9}$$

We assume that our quantity of interest can be expressed as a continuous[4] and linear[5] functional L. By recalling the linearity of L, we have

$$\text{Error of interest} = L(\mathbf{H}) - L(\mathbf{H}_{hp}) = L(\mathbf{H} - \mathbf{H}_{hp}) = L(\mathbf{e}), \tag{10}$$

where $\mathbf{e} = \mathbf{H} - \mathbf{H}_{hp}$ denotes the error function. By defining the residual $\mathbf{r}_{hp}$ belonging to the dual space of $\mathbf{V}$ (denoted by $\mathbf{V}'$) as $\mathbf{r}_{hp}(\mathbf{F}) = f(\mathbf{F}) - b(\mathbf{H}_{hp},\mathbf{F}) = b(\mathbf{H} - \mathbf{H}_{hp},\mathbf{F}) = b(\mathbf{e},\mathbf{F})$, we look for the solution of the *dual problem*

$$\begin{cases} \text{Find } \bar{\mathbf{W}} \in \mathbf{V} \\ b(\mathbf{F},\mathbf{W}) = L(\mathbf{F}) \quad \forall \mathbf{F} \in \mathbf{V}. \end{cases} \tag{11}$$

Problem (11) has a unique solution in $\mathbf{V}$. The solution $\mathbf{W}$, is usually referred to as the *influence function*.

[4] If the quantity of interest is not continuous, we may consider a continuous approximation L to the original quantity of interest.

[5] If the quantity of interest is represented by a non-linear functional, we linearize it around a specific solution, and replace the original functional L with its linearized version.

By discretizing (11) via, for example, $\mathbf{V}_{hp} \subset \mathbf{V}$, we obtain

$$\begin{cases} \text{Find } \bar{\mathbf{W}}_{hp} \in \mathbf{V}_{hp} \\ b(\mathbf{F}_{hp}, \mathbf{W}_{hp}) = L(\mathbf{F}_{hp}) \quad \forall \mathbf{F}_{hp} \in \mathbf{V}_{hp}. \end{cases} \tag{12}$$

Definition of the dual problem plus the Galerkin orthogonality for the original problem imply the final representation formula for the error in the quantity of interest, namely,

$$L(\mathbf{e}) = b(\mathbf{e}, \mathbf{W}) = b(\mathbf{e}, \underbrace{\mathbf{W} - \mathbf{F}_{hp}}_{\boldsymbol{\epsilon}}) = \tilde{b}(\mathbf{e}, \boldsymbol{\epsilon}).$$

At this point, $\mathbf{F}_{hp} \in \mathbf{V}_{hp}$ is arbitrary, and $\tilde{b}(\mathbf{e}, \boldsymbol{\epsilon}) = b(\mathbf{e}, \bar{\boldsymbol{\epsilon}})$ denotes the bilinear form corresponding to the original sesquilinear form.

Notice that, in practice, the dual problem is solved not for $\mathbf{W}$ but for its complex conjugate $\overline{\mathbf{W}}$ utilizing the bilinear form and *not* the sesquilinear form. The linear system of equations is factorized only once, and the extra cost of solving (12) reduces to only one backward and one forward substitution (if a direct solver is used).

Once the error in the quantity of interest has been determined in terms of bilinear form $\tilde{b}$, we wish to obtain a sharp upper bound for $|L(\mathbf{e})|$ that depends upon the mesh parameters (element size h and order of approximation p) *only locally*. Then, a self-adaptive algorithm intended to minimize this bound will be defined.

First, using a procedure similar to the one described in [16], we approximate $\mathbf{H}$ and $\mathbf{W}$ with *fine grid* functions $\mathbf{H}_{\frac{h}{2},p+1}$, $\mathbf{W}_{\frac{h}{2},p+1}$, which have been obtained by solving the corresponding linear system of equations associated with the FE subspace $\mathbf{V}_{\frac{h}{2},p+1}$. In the remainder of this article, $\mathbf{H}$ and $\mathbf{W}$ will denote the fine grid solutions of the direct and dual problems ($\mathbf{H} = \mathbf{H}_{\frac{h}{2},p+1}$, and $\mathbf{W} = \mathbf{W}_{\frac{h}{2},p+1}$, respectively), and we will restrict ourselves to discrete FE spaces only.

Next, we bound the error in the quantity of interest by a sum of element contributions. Let b_K denote a contribution from element K to sesquilinear form b. It then follows that:

$$|L(\mathbf{e})| = |b(\mathbf{e}, \boldsymbol{\epsilon})| \leqslant \sum_K |b_K(\mathbf{e}, \boldsymbol{\epsilon})|, \tag{13}$$

where summation over K indicates summation over elements.

2.3. Projection based interpolation operator

Once we have a representation formula for the error in the quantity of interest in terms of the sum of element contributions given by (13), we wish to express this upper bound in terms of local quantities, i.e. in terms of quantities that *do not* vary globally when we modify the grid locally. For this purpose, we introduce the idea of the *projection-based interpolation* operator. More precisely, we shall utilize the projection-based interpolation operator for *hp*-edge elements $\boldsymbol{\Pi}^{\text{curl}}_{hp} : \mathbf{V} \to \mathbf{V}_{hp}$ defined in [1]. This operator is local, it maintains conformity and it is optimal in the sense that the error behaves asymptotically, *both in h and p*, in the same way as the actual interpolation error (see [17] for details).

We shall also consider the Galerkin projection operator $\mathbf{P}^{\text{curl}}_{hp} : \mathbf{V} \to \mathbf{V}_{hp}$, and we will denote $\mathbf{H}_{hp} = \mathbf{P}^{\text{curl}}_{hp}\mathbf{H}$. Then, Eq. (13) becomes

$$\begin{aligned} |L(\mathbf{e})| &\leqslant \sum_K |b_K(\mathbf{e}, \boldsymbol{\epsilon})| \\ &= \sum_K |b_K(\mathbf{H} - \boldsymbol{\Pi}^{\text{curl}}_{hp}\mathbf{H}, \boldsymbol{\epsilon}) + b_K(\boldsymbol{\Pi}^{\text{curl}}_{hp}\mathbf{H} - \mathbf{P}^{\text{curl}}_{hp}\mathbf{H}, \boldsymbol{\epsilon})|. \end{aligned} \tag{14}$$

Given an element K, we conjecture that $|b_K(\boldsymbol{\Pi}^{\text{curl}}_{hp}\mathbf{H} - \mathbf{P}_{hp}\mathbf{H}, \boldsymbol{\epsilon})|$ will be negligible compared to $|b_K(\mathbf{H} - \boldsymbol{\Pi}^{\text{curl}}_{hp}\mathbf{H}, \boldsymbol{\epsilon})|$. Under this assumption, we conclude that

$$|L(\mathbf{e})| \preceq \sum_K |b_K(\mathbf{H} - \boldsymbol{\Pi}^{\text{curl}}_{hp}\mathbf{H}, \boldsymbol{\epsilon})|. \tag{15}$$

In particular, for $\boldsymbol{\epsilon} = \mathbf{W} - \boldsymbol{\Pi}^{\text{curl}}_{hp}\mathbf{W}$, we have

$$|L(\mathbf{e})| \preceq \sum_K |b_K(\mathbf{H} - \boldsymbol{\Pi}^{\text{curl}}_{hp}\mathbf{H}, \mathbf{W} - \boldsymbol{\Pi}^{\text{curl}}_{hp}\mathbf{W})|. \tag{16}$$

By applying Cauchy–Schwartz inequality, we obtain the next upper bound for $|L(\mathbf{e})|$

$$|L(\mathbf{e})| \preceq \sum_K \|\tilde{\mathbf{e}}\|_K \|\tilde{\boldsymbol{\epsilon}}\|_K, \tag{17}$$

where $\tilde{\mathbf{e}} = \mathbf{H} - \boldsymbol{\Pi}^{\text{curl}}_{hp}\mathbf{H}$, $\tilde{\boldsymbol{\epsilon}} = \mathbf{W} - \boldsymbol{\Pi}^{\text{curl}}_{hp}\mathbf{W}$, and $\|\cdot\|_K$ denotes energy-norm $\|\cdot\|$ restricted to element K.

2.4. Goal-oriented hp-mesh optimization algorithm

We describe a self-adaptive goal-oriented *hp* algorithm that utilizes the main ideas of the fully automatic (energy-norm based) *hp*-adaptive algorithm described in [16,18,1]. The goal-oriented mesh optimization algorithm iterates along the following steps.

- **Step 0**: Compute the upper-bound estimate of the coarse grid approximation error in the quantity of interest. This estimate is computed using Eq. (17). If the difference is smaller than a user-prescribed error tolerance, then we deliver the fine mesh solution as our final answer, and we stop the execution of our algorithm.
- **Step 1**: For each edge in the coarse grid, compute the error decrease rate for the p refinement, and all possible h-refinements. Let p_1, p_2 be the order of the edge sons in the case of h-refinement. Then, we compute

$$\text{Error decrease}(\hat{hp}) = \sum_K \left[\frac{\|\mathbf{H} - \boldsymbol{\Pi}^{\text{curl}}_{hp}\mathbf{H}\|_K \cdot \|\mathbf{W} - \boldsymbol{\Pi}^{\text{curl}}_{hp}\mathbf{W}\|_K}{(p_1 + p_2 - p)} - \frac{\|\mathbf{H} - \boldsymbol{\Pi}^{\text{curl}}_{\hat{hp}}\mathbf{H}\|_K \cdot \|\mathbf{W} - \boldsymbol{\Pi}^{\text{curl}}_{\hat{hp}}\mathbf{W}\|_K}{(p_1 + p_2 - p)} \right], \tag{18}$$

where $\widehat{hp} = (\hat{h}, \hat{p})$ is such that $\hat{h} \in \{h, h/2\}$. If $\hat{h} = h$, then $\hat{p} = p + 1$. If $\hat{h} = h/2$, then $\hat{p} = (p_1, p_2)$, where $p_1 + p_2 - p > 0$, $\max\{p_1, p_2\} \leqslant p + 1$.

Steps 0 and 1 described above are analogous to those presented in [1] for energy-norm *hp*-adaptivity. The remaining steps (2–5) are exactly the same as those described in [1].

Remark. If functional L describing the quantity of interest is equal to the load f of the original (direct) problem, then $\mathbf{H} = \mathbf{W}$, and the goal-oriented algorithm described above is identical with the energy-norm algorithm presented in [1].

Similarities between the energy norm based *hp*-adaptivity and the goal-oriented *hp*-adaptivity are well reflected in the corresponding implementation. The latter one is simply an extension of the first one.

2.5. Implementation details

In what follows, we discuss the main implementation details needed to extend the fully automatic (energy-norm based) *hp*-adaptive algorithm [16,18] to a fully automatic goal-oriented *hp*-adaptive algorithm.

(1) First, solution $\mathbf{W}$ of the dual problem on the fine grid is necessary. This goal can be attained either by using a direct (frontal) solver or an iterative (two-grid) solver (see [19]).
(2) Subsequently, we should treat both solutions as satisfying two different partial differential equations (PDE's). We select functions $\mathbf{H}$ and $\mathbf{W}$ as the solutions of the system of two PDE's.
(3) We proceed to redefine the evaluation of the error. The energy-norm error evaluation of a two-dimensional function is replaced by the product $\|\mathbf{H} - \mathbf{\Pi}^{\text{curl}}_{hp}\mathbf{H}\| \cdot \|\mathbf{W} - \mathbf{\Pi}^{\text{curl}}_{hp}\mathbf{W}\|$.
(4) After these simple modifications, the energy-norm based self-adaptive algorithm may now be utilized as a self-adaptive goal-oriented *hp* algorithm.

3. Numerical results

In this section, we use three different methods.

- The fully automatic energy-norm based *hp*-adaptive strategy described in [1],
- a mode matching technique [13], and
- the fully automatic goal-oriented *hp*-adaptive strategy described in Section 3.1.

The methods are applied to a fifth-order filter consisting on a H-plane structure with six symmetric inductive irises (as the one analyzed in the first paper). This is a challenging problem with 24 singularities.

Then, results are compared against each other, and the main advantages and disadvantages of each methodology are discussed.

3.1. A rectangular waveguide structure with six inductive irises

We consider a six inductive irises filter[6] of dimensions $\approx 20 \times 2 \times 1$ cm, operating in the range of frequencies $\approx$8.8–9.6 GHz. More precisely, our computational domain is given by $\Omega = \Omega_1 - (\Omega_2 \cup \Omega_3 \cup \Omega_4 \cup \Omega_5 \cup \Omega_6 \cup \Omega_7)$, where:

- $\Omega_1 = \{(x, y, z) : 0\text{ cm} \leqslant x \leqslant 20.2913\text{ cm},\ -1.143\text{ cm} \leqslant y \leqslant 1.143\text{ cm},\ 0\text{ cm} \leqslant z \leqslant 1.016\text{ cm}\}$,
- $\Omega_2 = \{(x, y, z) : 5\text{ cm} \leqslant x \leqslant 5.2\text{ cm},\ -1.143\text{ cm} \leqslant y \leqslant -0.7191\text{ cm},\ 0\text{ cm} \leqslant z \leqslant 1.016\text{ cm}\} \cup \{(x, y, z) : 5\text{ cm} \leqslant x \leqslant 5.2\text{ cm}, 0.7191\text{ cm} \leqslant y \leqslant 1.143\text{ cm}, 0\text{ cm} \leqslant z \leqslant 1.016\text{ cm}\}$,
- $\Omega_3 = \{(x, y, z) : 6.8641\text{ cm} \leqslant x \leqslant 7.0641\text{ cm},\ -1.143\text{ cm} \leqslant y \leqslant -0.54975\text{ cm}, 0\text{ cm} \leqslant z \leqslant 1.016\text{ cm}\} \cup \{(x, y, z) : 6.8641\text{ cm} \leqslant x \leqslant 7.0641\text{ cm},\ 0.54975\text{ cm} \leqslant y \leqslant 1.143\text{ cm},\ 0\text{ cm} \leqslant z \leqslant 1.016\text{ cm}\}$,
- $\Omega_4 = \{(x, y, z) : 8.9702\text{ cm} \leqslant x \leqslant 9.1702\text{ cm},\ -1.143\text{ cm} \leqslant y \leqslant -0.5078\text{ cm},\ 0\text{ cm} \leqslant z \leqslant 1.016\text{ cm}\} \cup \{(x, y, z) : 8.9702\text{ cm} \leqslant x \leqslant 9.1702\text{ cm},\ 0.5078\text{ cm} \leqslant 1.143\text{ cm},\ 0\text{ cm} \leqslant z \leqslant 1.016\text{ cm}\}$,
- $\Omega_5 = \{(x, y, z) : 11.1211\text{ cm} \leqslant x \leqslant 11.3211\text{ cm},\ -1.143\text{ cm} \leqslant y \leqslant -0.5078\text{ cm},\ 0\text{ cm} \leqslant z \leqslant 1.016\text{ cm}\} \cup \{(x, y, z) : 11.1211\text{ cm} \leqslant x \leqslant 11.3211\text{ cm}, 0.5078\text{ cm} \leqslant y \leqslant 1.143\text{ cm}, 0\text{ cm} \leqslant z \leqslant 1.016\text{ cm}\}$,
- $\Omega_6 = \{(x, y, z) : 13.2272\text{ cm} \leqslant x \leqslant 13.4272\text{ cm},\ -1.143\text{ cm} \leqslant y \leqslant -0.54975\text{ cm},\ 0\text{ cm} \leqslant z \leqslant 1.016\text{ cm}\} \cup \{(x, y, z) : 13.2272\text{ cm} \leqslant x \leqslant 13.4272\text{ cm}, 0.54975\text{ cm} \leqslant y \leqslant 1.143\text{ cm}, 0\text{ cm} \leqslant z \leqslant 1.016\text{ cm}\}$, and,
- $\Omega_7 = \{(x, y, z) : 15.0913\text{ cm} \leqslant x \leqslant 15.2913\text{ cm},\ -1.143\text{ cm} \leqslant y \leqslant -0.7191\text{ cm},\ 0\text{ cm} \leqslant z \leqslant 1.016\text{ cm}\} \cup \{(x, y, z) : 15.0913\text{ cm} \leqslant x \leqslant 15.2913\text{ cm}, 0.7191\text{ cm} \leqslant y \leqslant 1.143\text{ cm}, 0\text{ cm} \leqslant z \leqslant 1.016\text{ cm}\}$.

The geometry is shown in Fig. 1. The structure consists of five cavities acting as resonators coupled by themselves and with the waveguide sections by means of the irises. Thus, a selective frequency response can be adjusted by a careful choice of the size of the cavities and the irises. Specifically, the structure has been designed to work as a band-pass filter in the 8.8–9.6 GHz frequency range (see Fig. 3 in the section on numerical results).

3.2. Results obtained by using the energy-norm hp-adaptive strategy

First, we solve our waveguide problem using the fully automatic *hp*-adaptive strategy. In order to construct an

[6] We thank Mr. Sergio Llorente for designing the waveguide filter structure.

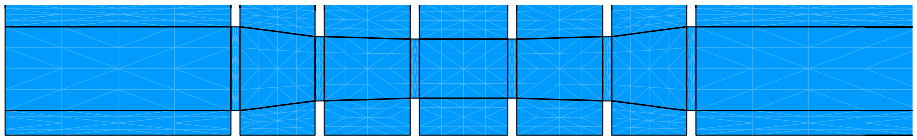

Fig. 1. 2D cross-section of the geometry of the waveguide problem with six inductive irises. The initial grid is composed of 27 elements, as indicated by the black lines.

adequate initial grid for our adaptive algorithm, we notice the following limitation:

- *We cannot guarantee the optimality of the fully automatic hp-adaptive strategy if the dispersion error is large, which may occur in the pre-asymptotic regime.* Since solution of the problem on the fine grid is used to guide optimal *hp*-refinements, we need to control the dispersion error on the fine grid. Thus, h needs to be sufficiently small or p sufficiently large. Otherwise, convergence results in the pre-asymptotic regime may not look as expected.

In Fig. 2, we compare the convergence history obtained by using the fully automatic *hp*-adaptive strategy starting with different initial grids. For third-order elements, the dispersion error is under control (see estimates of [20–22]), and the fully automatic *hp*-adaptive strategy converges exponentially from the beginning, as indicated by a straight line in the algebraic vs logarithmic scales. We also observe that, in the asymptotic regime, all curves present similar rates of convergence. These results indicate that the choice of initial grid is not very important and, even in the case of very coarse initial grids, the algorithm will eventually notice the asymptotic behavior of the solution, and the overall convergence will be exponential.

We solved the six irises waveguide problem delivering a 0.3% relative error in the energy-norm. Fig. 3 displays the magnitude of the S_{11} scattering parameter (on the decibel scale) with respect to the frequency. This quantity is usually

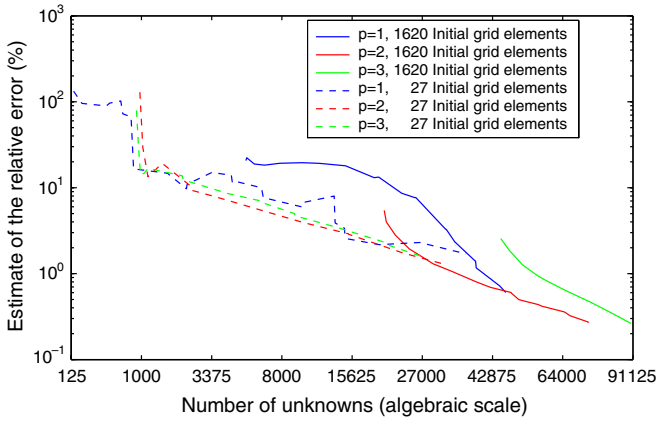

Fig. 2. Convergence history using the fully automatic *hp*-adaptive strategy for different initial grids. Different colors correspond to different initial order of approximation. Twenty-seven is the minimum number of elements needed to reproduce the geometry, while 1620 is the minimum number of elements needed to reproduce the geometry and to guarantee convergence of the iterative two grid solver described in [19].

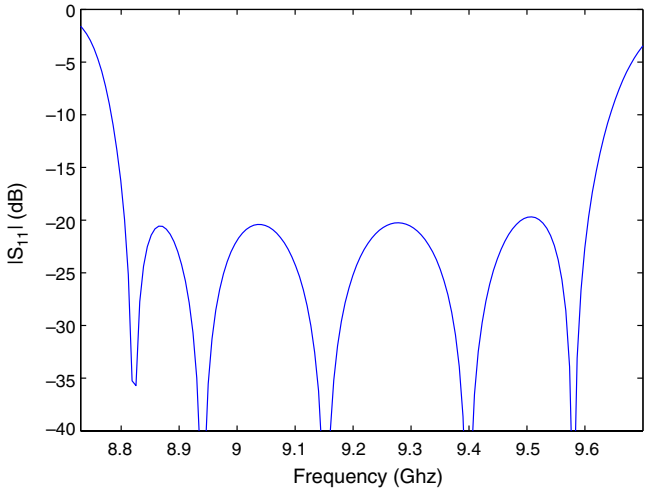

Fig. 3. Return loss of the waveguide structure.

referred to as the return loss of the waveguide structure, and it is given by Eq. (19), see [1]

$$S_{11} = \frac{\int_{\Gamma_1} \mathbf{H}(\xi) \cdot \sin\frac{\pi\xi}{a}\, \mathrm{d}S}{\mathbf{H}^{\mathrm{in}}\frac{a}{2}} - 1, \tag{19}$$

where a is the size of the excitation port. For the frequency interval 8.8–9.6 GHz, the return loss is below -20 dB, which indicates that almost all energy passes through the structure, and thus, the waveguide acts as a bandpass filter. The other scattering parameter of interest is S_{21} (S_{12} and S_{22} are obtained using (3) and (4), respectively) which is given in Eq. (20), see also [1].

$$S_{21} = \frac{\int_{\Gamma_2} \mathbf{H}(\xi) \cdot \sin\frac{\pi\xi}{a}\, \mathrm{d}S}{\mathbf{H}^{\mathrm{in}}\frac{a}{2}}. \tag{20}$$

Figs. 4–7 display solution at different frequencies. For frequencies 8.72 GHz, and 9.71 GHz, the return loss of the waveguide structure is large, and for frequencies 8.82 GHz, and 9.58 GHz the return loss is below -20 dB.

3.3. Results obtained by using a Mode Matching technique

In this subsection, we solve our problem of interest with a Mode Matching technique. More precisely, we compute the S-parameters by using the software available in [13]. In Fig. 8, we display the S-parameters as a function of frequency. Notice the similarities of these results with those presented in Fig. 3.

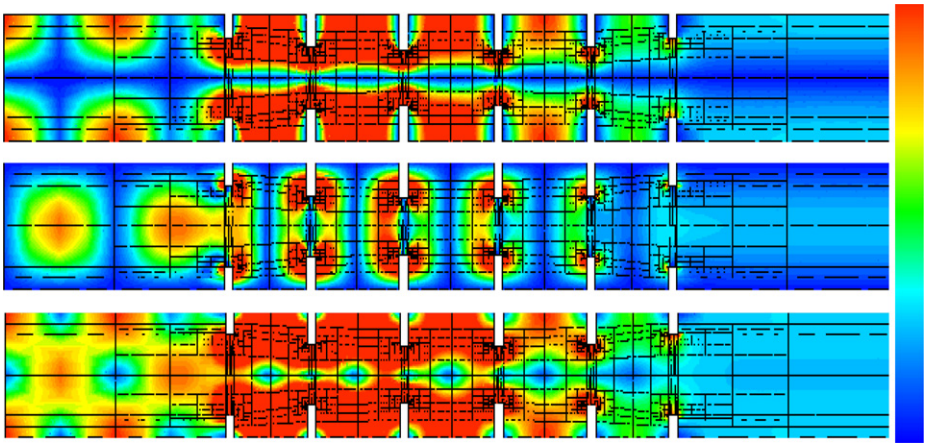

Fig. 4. $|H_x|$ (upper figure), $|H_y|$ (center figure), and $\sqrt{|H_x|^2 + |H_y|^2}$ (lower figure) at 8.72 GHz for the six irises waveguide problem.

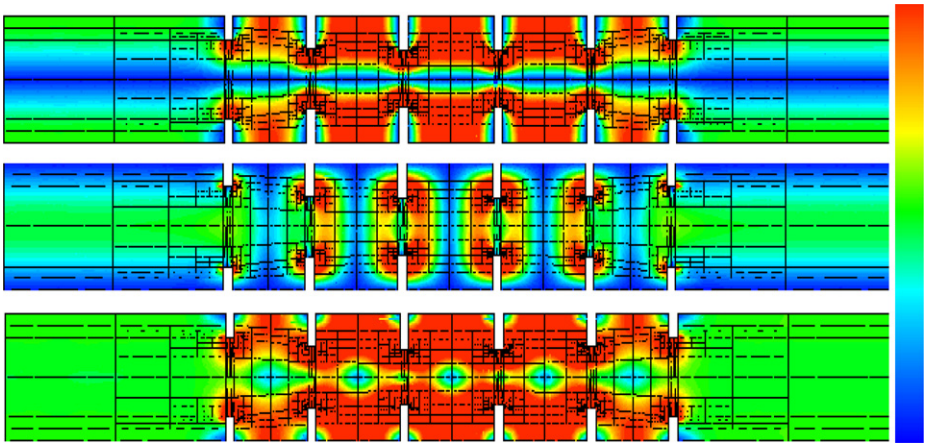

Fig. 5. $|H_x|$ (upper figure), $|H_y|$ (center figure), and $\sqrt{|H_x|^2 + |H_y|^2}$ (lower figure) at 8.82 GHz for the six irises waveguide problem.

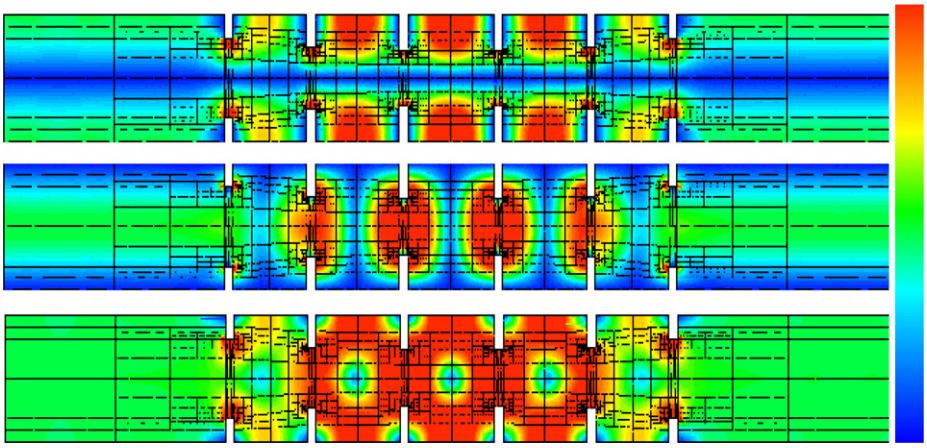

Fig. 6. $|H_x|$ (upper figure), $|H_y|$ (center figure), and $\sqrt{|H_x|^2 + |H_y|^2}$ (lower figure) at 9.58 GHz for the six irises waveguide problem.

3.4. Results obtained by using the goal-oriented hp-adaptive strategy

The final *hp*-grid delivered by the fully automatic, energy-norm based adaptive algorithm is expected to produce a "reasonably good" approximation of the exact solution almost *everywhere in the computational domain*. Thus, we may decide what quantity to compute (for example, the S_{11} parameter) after solving the problem.

However, when using the goal-oriented *hp*-adaptivity, we need to decide first what quantity is of interest for us (for example, S_{11}), and then construct a grid intended to obtain the best possible approximation of that quantity of interest with respect to the problem size. Notice that

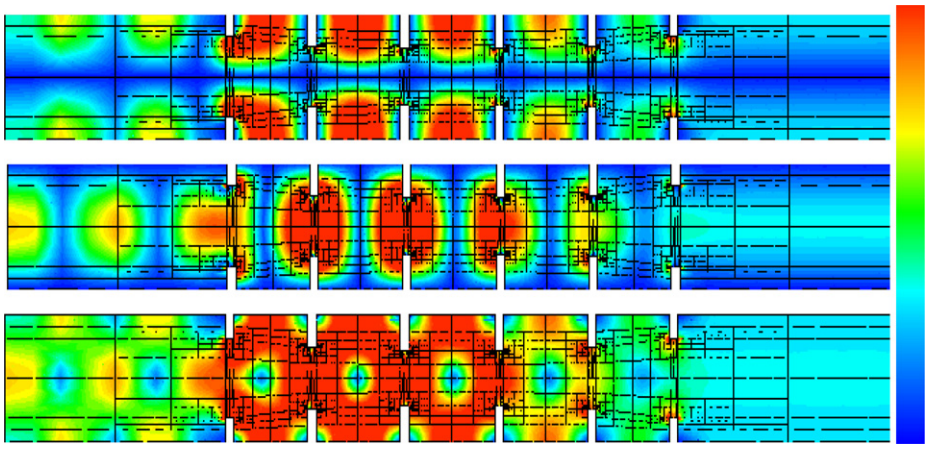

Fig. 7. $|H_x|$ (upper figure), $|H_y|$ (center figure), and $\sqrt{|H_x|^2+|H_y|^2}$ (lower figure) at 9.71 GHz for the six irises waveguide problem.

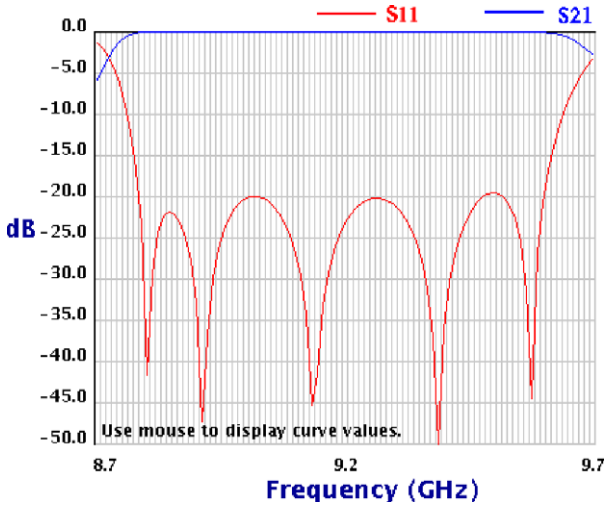

Fig. 8. Return loss of the waveguide structure. This graph has been computed using a Mode Matching technique [13].

quality of the solution *everywhere else* in the domain may be poor.

We note that it is possible to define a single quantity of interest relating different S-parameters. Thus, an accurate solution in the quantity of interest will imply accuracy of several S-parameters simultaneously (multiple goals). However, it is unclear for these authors how to optimally select such a quantity of interest. For example, if we select the sum of different S-parameters, then the goal-oriented algorithm will first approximate the S-parameters with higher value. Perhaps a weighted sum of the S-parameters is an adequate selection for the quantity of interest, where the weights are inversely proportional to the values of the S-parameters. For details on multi-goal oriented adaptivity, see [23].

Thus, we revisit the question on which of the S-parameters should be computed. For instance, will it be better to directly compute S_{11}, or to compute S_{21} and then apply identity (5) to obtain S_{11}? These questions are especially important when considering goal-oriented adaptive algorithms, since the configuration of the final grid will depend upon the quantity of interest (S-parameter) that we select before refinements.

In order to select between the four different S-parameters relevant to our waveguide structure, we first notice that at the discrete level (when considering finite element approximation), identity (3) is also valid due to the fact that reciprocity is also satisfied at the discrete level. Thus, the use of the goal-oriented adaptivity with S_{12} or S_{21} as our quantity of interest will provide identical grids and results. However, identity (4) will hold at the discrete level only if the grid is symmetric. Since in this paper we are considering symmetrical initial grids, the goal-oriented adaptive algorithm with S_{11} or S_{22} as our quantity of interest will provide identical grids and results. Finally, notice that identity (5) will *not hold* in general at the discrete level, even if the grid is symmetric. In summary, we shall consider two different quantities of interest,

(1) $L_1(\mathbf{H}) := S_{11}(\mathbf{H}) + 1$,[7] and
(2) $L_2(\mathbf{H}) := S_{21}(\mathbf{H})$.

Then, we will numerically study the self-adaptive goal-oriented *hp*-adaptive strategy by executing it twice: first, using L_1 as our quantity of interest, and then considering L_2 as our quantity of interest. Finally, in order to compare the results, we will use for the second case (L_2) Eq. (5) in order to post-process $S_{11}(\mathbf{H}) + 1$ from $S_{21}(\mathbf{H})$.

Convergence results are displayed in Fig. 9 at different frequencies: 8.72 GHz (top-left panel), 8.82 GHz (top-right panel), 9.58 GHz (bottom-left panel), and 9.71 GHz (bottom-right panel). These frequencies correspond to solutions shown in Figs. 4–7, respectively. The red curve displays the relative error in percentage of $S_{11} + 1$ with respect to the number of unknowns, when executing the goal-oriented *hp*-adaptive algorithm with L_1 as our quantity of interest. If we consider L_2 as our quantity of interest,

[7] Notice that $S_{11}(\mathbf{H})$ is not a linear functional. However, $S_{11}(\mathbf{H}) + 1$ is a linear and continuous functional, and therefore, we may use it as our quantity of interest for the goal-oriented optimization algorithm.

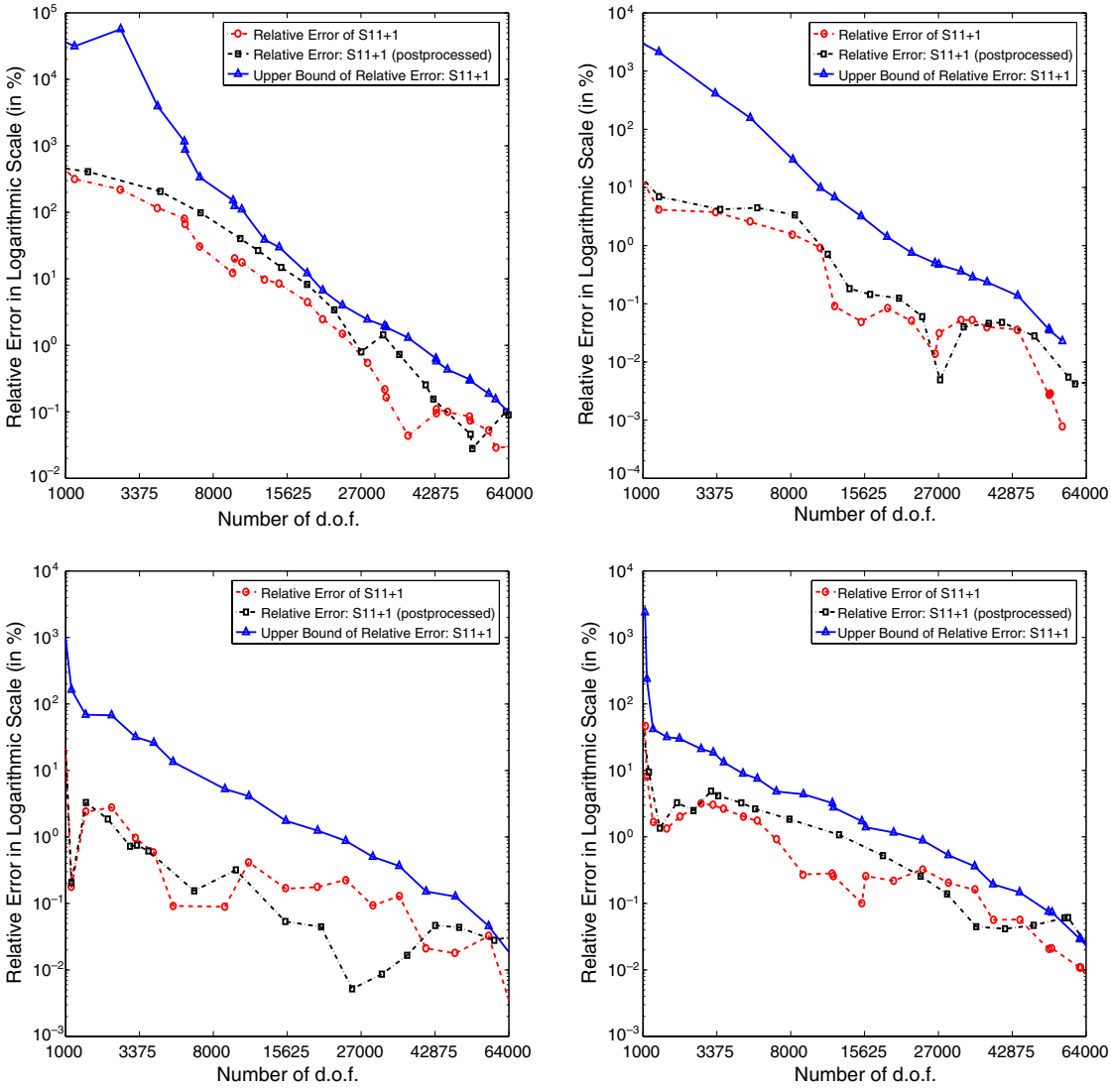

Fig. 9. Convergence history for the waveguide problem with six inductive irises at different frequencies: 8.72 GHz (top-left panel), 8.82 GHz (top-right panel), 9.58 GHz (bottom-left panel), and 9.71 GHz (bottom-right panel). The red and black curves display the relative error in percentage of $S_{11}+1$ with respect to the number of unknowns, when executing the goal-oriented *hp*-adaptive algorithm with L_1 and L_2 as our quantity of interest, respectively. The blue curve corresponds to upper bound (17) used for minimization, when considering $|L_1(\mathbf{H})|$ as our quantity of interest.

the corresponding relative error of $S_{11}+1$ – computed using (5) – is displayed by the black curve. Finally, the blue curve corresponds to upper bound (17) used for minimization, when considering $|L_1(\mathbf{H})|$ as our quantity of interest.

From results of Fig. 9, we conclude the following.

- The self-adaptive goal-oriented *hp*-FEM delivers exponential converges rates in terms of upper bound (17) of quantity of interest $|L_1(\mathbf{H})|$ against the problem size (number of d.o.f.), as indicated by the straight line (blue curve) in the algebraic (number of d.o.f. to the power of 1/3) vs. logarithmic scale.
- Since the blue curve converges exponentially, and it is an upper bound estimate of the red curve, the latter curve should also display an overall exponential convergence behavior (or at least it is bounded by a curve that exponentially converges to zero), regardless of the fact that the error in the quantity of interest may temporary increase when executing the refinements.
- The final relative error in the quantity of interest remains below 0.1% in all cases.
- To utilize quantity of interest L_2 as opposed to L_1 (or vice-versa) for executing the goal-oriented adaptive algorithm is not essential for this problem. Numerical results are similar in both cases.

3.5. A comparison between the energy-norm and goal-oriented self-adaptive hp-FE strategies

Quantity of interest L_1 is equal (up to a multiplicative constant) to the functional f representing the right hand side of the original problem. Thus, solution of the dual

problem **W** is also equal (up to a multiplicative constant) to the solution of the original problem **H**. For this particular case, the goal-oriented adaptivity coincides exactly with the energy driven adaptivity, and the corresponding numerical results are identical. In other words, for this particular waveguide problem, energy-norm adaptivity is optimal for approximating L_1.

On the other hand, if we are interested in computing S_{21}, then results obtained from the goal-oriented algorithm are different from those obtained with energy-norm adaptivity. Nevertheless, Fig. 9 illustrates that the results coming from both algorithms, although different, are quite similar to each other, since S_{21} is also strongly related to the energy of the solution.

Differences between energy-norm adaptivity and goal-oriented adaptivity shall become larger as we consider resistive materials and/or more complex waveguide structures with possibly several ports, in which the quantity of interest is not strongly related to the conservation of energy. To illustrate this effect, we consider our original problem with the three central cavities filled by a lossy material (see Fig. 10) with $\epsilon = \epsilon_0\epsilon_r$, where $\epsilon_0 = 8.854 * 10^{-12}$ F/m is the permittivity of the vacuum, and $\epsilon_r = (1 - 0.07805\mathrm{j}/(\omega\epsilon_0))$. Results at 8.82 GHz, i.e. $\epsilon_r = (1 - \mathrm{j}/(2\pi))$ are displayed in Fig. 11. When the goal of computations is to approximate S_{11}, the grid obtained with the goal-oriented adaptivity for $S_{11} + 1$ provides results that are one order of magnitude more accurate than those obtained with the goal-oriented adaptivity and S_{21} as our quantity of interest. If the goal of computations is to approximate S_{21}, the grid obtained with the goal-oriented adaptivity for S_{21} provides results that are up to 500 times more accurate than those obtained with the goal-oriented adaptivity and $S_{11} + 1$ as our quantity of interest. Since grids obtained from using the goal-oriented adaptivity for $S_{11} + 1$ are equal to those obtained from using energy-norm adaptivity, we conclude that the goal-oriented adaptivity for S_{21} provides approximations to S_{21} that are far more accurate than those obtained with the energy-norm adaptivity. Eventually, for a resistive enough material, the use of goal-oriented adaptivity will become essential (see [10,11] for details) for accurately approximating S_{21}.

Two *hp*-grids for our original problem with the three central cavities filled by a lossy material are shown in Fig. 12. The two *hp*-grids displayed in Fig. 12 are essentially different:

(1) The top panel displays a grid obtained by using L_1 as our quantity of interest. Therefore, we observe severe refinements towards the excitation (left) port.

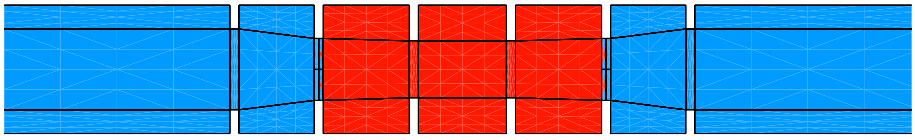

Fig. 10. 2D cross-section of the geometry of the waveguide problem with six inductive irises. The red color indicates that the three central cavities are filled with a resistive material.

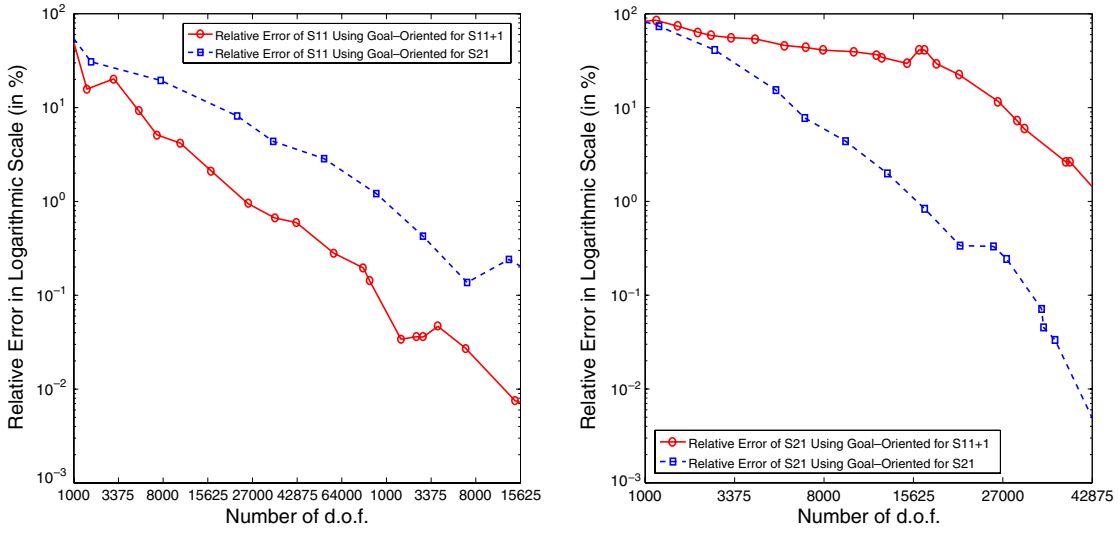

Fig. 11. Convergence history for the waveguide problem with six inductive irises at 8.82 GHz, with the three central cavities filled with a resistive material. The left panel describes the convergence history for S_{11}, and the right panel for S_{21}. The blue curves have been obtained by using goal-oriented adaptivity with S_{21} as our quantity of interest, and the red curves by using goal-oriented adaptivity with $S_{11} + 1$ as our quantity of interest.

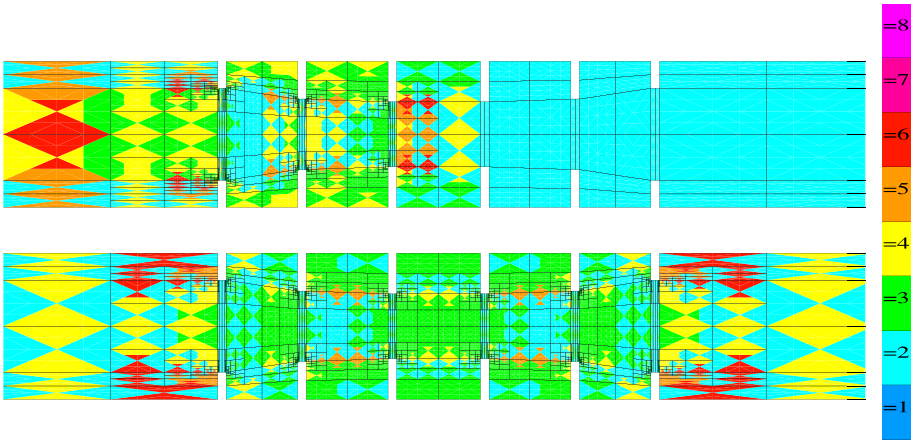

Fig. 12. *hp*-grids obtained by using the fully automatic goal-oriented *hp*-adaptive finite element method with $S_{11}+1$ (top panel) and S_{21} (bottom panel) as our quantities of interest, respectively. Different colors indicate different polynomials orders of approximation, ranging from 1 (dark blue) up to 8 (pink). The *hp*-grids contain 12110 (top) and 13054 (bottom) unknowns, respectively.

(2) The bottom panel displays a grid obtained by using L_2 as our quantity of interest. In this case, we obtain a symmetric grid with several refinements towards both the excitation (left) and the output (right) ports.

Notice that the final mesh is symmetric with respect to the center of the waveguide structure because the initial grid is symmetric and the upper bound $\sum_K |b_K(\mathbf{e},\boldsymbol{\epsilon})|$, used for the minimization, is also symmetric since solutions of the original and dual problems are symmetric with respect to each other (up to a constant).

To summarize, the energy-norm adaptivity can be seen as a particular case of the goal-oriented adaptivity. For the waveguide problem that we are considering in this paper, results for (the particular case of) energy-norm adaptivity are close to optimal. Indeed, they are exactly optimal if we consider L_1 as our quantity of interest. Thus, there is no need to use the goal-oriented adaptivity for this problem. Nevertheless, it is important to realize that for some other problems (for instance, waveguide problems with lossy media, or waveguide problems with several ports), the use of goal-oriented adaptivity may become essential. In any case, results coming from the goal-oriented adaptivity should never be worse than those obtained with the energy-norm adaptivity.

4. Conclusions

In this paper, a fully automatic goal-oriented *hp*-FEM has been presented for the analysis of rectangular waveguide discontinuities. A challenging problem containing six inductive irises (24 singularities) in the H-plane has been solved.

Numerical results indicate that,

- the method converges exponentially (regardless of the initial grid used),
- accuracy of the method is comparable to that obtained with a Mode Matching (semi-analytical) technique, and at the same time, the finite element method allows for modeling of more complex waveguide structures,
- the goal-oriented adaptivity is a generalization of the energy-norm adaptivity which may (or may not) be essential in order to accurately solve a problem, and,
- from the physical point of view, the waveguide acts as a bandpass filter.

Summarizing the two papers we conclude the following. A relevant microwave engineering problem involving the analysis of H-plane and E-plane rectangular waveguide discontinuities (and the computation of their *S*-parameters), has been solved by using a fully automatic *hp*-adaptive FEM. The *hp* adaptivity has been shown to deliver exponential convergence rates for the error, even in the presence of singularities, for a wide variety of relevant structures including microwave engineering devices of medium complexity. While keeping the advantage of being a purely numerical method, the *hp*-adaptivity has shown to be more accurate than semi-analytical techniques. The suitability of a goal-oriented approach in terms of the *S*-parameters, in comparison with a "conventional" approach in terms of energy-norm, has been clarified.

References

[1] L.E. García-Castillo, D. Pardo, I. Gómez-Revuelto, L.F. Demkowicz, A two-dimensional self-adaptive *hp*-adaptive finite element method for the characterization of waveguide discontinuities. Part I: Energy-norm based automatic *hp*-adaptivity, Comput. Methods Appl. Mech. Engrg., in press, doi:10.1016/j.cma.2007.06.024.

[2] N. Marcuvitz, Waveguide Handbook, IEE, 1985.

[3] J. Uher, J. Bornemann, U. Rosenberg, Waveguide Components for Antenna Feed Systems: Theory and CAD, Artech House Publishers, Inc., 1993.

[4] J. Oden, S. Prudhomme, Goal-oriented error estimation and adaptivity for the finite element method, Comput. Math. Appl. 41 (5–6) (2001) 735–756.

[5] S. Prudhomme, J. Oden, On goal-oriented error estimation for elliptic problems: application to the control of pointwise errors, Comput. Methods Appl. Mech. Engrg. 176 (1–4) (1999) 313–331.

[6] R. Becker, R. Rannacher, Weighted a posteriori error control in FE methods, in: Hans Georg Bock et al. (Eds.), ENUMATH 97. Proceedings of the 2nd European Conference on Numerical Mathematics and Advanced Applications held in Heidelberg, Germany, September 28–October 3, 1997. Including a selection of papers from the 1st Conference (ENUMATH 95) held in Paris, France, September 1995. World Scientific, Singapore, 1998, pp. 621–637.
[7] V. Heuveline, R. Rannacher, Duality-based adaptivity in the *hp*-finite element method, J. Numer. Math. 11 (2) (2003) 95–113.
[8] M. Paraschivoiu, A.T. Patera, A hierarchical duality approach to bounds for the outputs of partial differential equations, Comput. Methods Appl. Mech. Engrg. 158 (3–4) (1998) 389–407.
[9] R. Rannacher, F. Suttmeier, A posteriori error control in finite element methods via duality techniques: application to perfect plasticity, Comput. Mech. 21 (2) (1998) 123–133.
[10] D. Pardo, L. Demkowicz, C. Torres-Verdin, L. Tabarovsky, A goal oriented *hp*-adaptive finite element method with electromagnetic applications. Part I: Electrostatics, Int. J. Numer. Methods Engrg. 65 (8) (2006) 1269–1309, see also ICES Report 04-57.
[11] D. Pardo, L. Demkowicz, C. Torres-Verdin, M. Paszynski, Simulation of resistivity logging-while-drilling (LWD) measurements using a self-adaptive goal-oriented *hp*-finite element method, SIAM J. Appl. Math. 66 (6) (2006) 2085–2106.
[12] M. Paszynski, L. Demkowicz, D. Pardo, Verification of goal-oriented *hp* adaptivity, Comput. Math. Appl. 50 (8–9) (2005) 1395–1404, see also ICES Report 05-06.
[13] www.guidedwavetech.com, Guided wave technology, 2004.
[14] T. Itoh, Numerical Techniques for Microwave and Millimeter Wave Passive Structures, John Wiley & Sons, Inc., 1989.
[15] L.F. Demkowicz, Encyclopedia of Computational Mechanics, John Wiley & Sons, Inc., 2004 (Chapter "Finite element methods for Maxwell equations").
[16] L. Demkowicz, W. Rachowicz, P. Devloo, A fully automatic *hp*-adaptivity, J. Sci. Comput. 17 (1–4) (2002) 117–142.
[17] L.F. Demkowicz, A. Buffa, H^1, H(curl) and H(div)-conforming projection-based interpolation in three dimensions. Quasi optimal *p*-interpolation estimates, Comput. Methods Appl. Mech. Engrg. 194 (24) (2005) 267–296, see also ICES Report 04-24.
[18] W. Rachowicz, D. Pardo, L.F. Demkowicz, Fully automatic *hp*-adaptivity in three dimensions, Comput. Methods Appl. Mech. Engrg. 195 (37–40) (2006) 4186–4842.
[19] D. Pardo, Integration of *hp*-adaptivity with a two grid solver: applications to electromagnetics, Ph.D. thesis, The University of Texas at Austin, April 2004.
[20] M. Ainsworth, Discrete dispersion relation for *hp*-version finite element approximation at high wave number, SIAM J. Numer. Anal. 42 (2) (2004) 553–575.
[21] F. Ihlenburg, I. Babuska, Finite element solution of the Helmholtz equation with high wave number. I: The *h*-version of the FEM., Comput. Math. Appl. 30 (9) (1995) 9–37.
[22] F. Ihlenburg, I. Babuska, Finite element solution of the Helmholtz equation with high wave number. II: The *h*–*p* version of the FEM, SIAM J. Numer. Anal. 34 (1) (1997) 315–358.
[23] R. Hartmann, P. Houston, Hyperbolic Problems: Theory, Numerics, Applications, Springer, 2003, pp. 579–588 (Chapter "Goal-oriented. A posteriori error estimation for multiple target functionals").